University of Baghdad
College of Engineering
JOURNAL OF ENGINEERING

Journal of Engineering
journal homepage: www.jcoeng.edu.iq
Volume 31 Number 6 June 2025

Numerical Study of Convective Heat Transfer in a Rectangular Channel Inserted with Metal Foam of Gradient Pore Density

Mohammed H. Hasan *, **Raed G. Saihood**

Department of Mechanical Engineering, College of Engineering, University of Baghdad, Baghdad, Iraq

ABSTRACT

Metal foam has recently been used in many engineering applications, such as solar collectors, heat exchangers, and cooling of electronic devices, which calls for studying different cases of using metal foam in these applications. The current study conducts a numerical analysis of heat transfer and fluid flow characteristics for air in a rectangular channel filled with high-porosity copper foam. The study examined the thermal performance for two cases of gradient pore density, which are arranged as (10-20-40) PPI and (40-20-10) PPI. These cases were compared with two other cases for constant pore density, 10 and 40 PPI, and empty cases. The ANSYS FLUENT 20.0 employed the Darcy-Forchheimer extended Brickman model in the two-dimensional domain with the local thermal non-equilibrium model (LTNE) for the energy equation to obtain the numerical simulation for this study. The working parameters included air with Re from 200 to 2100 and applied heat flux from 450 to 6000 W/m^2. The results indicated that employing metal foam with a low pore density led to a decrease in both the Nusselt number and pressure drop. Both gradient cases exhibited Nusselt numbers and friction factors that fell within the range of the constant PPI cases, but one of the gradient cases increased the performance factor by 10%. In general, the PPI configuration of 10-20-40 exhibited a higher heat transfer coefficient in comparison to the 40-20-10 PPI arrangement with the same pressure drop.

Keywords: Convection, Gradient, Metal foam, Pore per inch, Rectangular.

1. INTRODUCTION

Several fundamental theories describe how to enhance heat transfer in internal flow. These theories play a major role in industrial and technical applications, helping to save energy and minimize expenses associated with construction and operation. Different methods, such as the use of porous media, are employed. One of the porous media used is metal foam, which can be made of different types of metals depending on their thermal conductivity, such as

*Corresponding author
Peer review under the responsibility of University of Baghdad.
https://doi.org/10.31026/j.eng.2025.06.07
© 2025 The Author(s). Published by the College of Engineering, University of Baghdad
This is an open access article under the CC BY 4 license (http://creativecommons.org/licenses/by/4.0/).
Article received: 07/11/2024
Article revised: 29/12/2024
Article accepted: 28/01/2025
Article published: 01/06/2025

copper, aluminum, and nickel. The properties of metal foam include reducing the boundary layer resistance, reducing the transition region between laminar and turbulent flow, and increasing the contact area between the hot surface and working fluid, depending on the number of pores per inch. One common strategy is to increase the surface area of the channel wall **(Xu et al., 2011; Akbar et al., 2024).** Over the past 20 years, a variety of research projects have shown an interest in cells of metal foam with high porosity because it has special properties, such as having different pore densities and being lightweight **(Kopanidis et al., 2010; Sener et al., 2016; Ali and Rasheed, 2024)**. This technique provides a large surface area with high thermal conductivity, but it needs more pumping power. Metal foam has potential applications in filters, nuclear reactor cooling, chemical reactors, combustion chambers, reformers, biomedical implants, compact heat sinks, and heat exchangers. **(Qu et al., 2012; Shokouhmand and Emami, 2012; Rasheed and Abood, 2017).**

(Lu et al., 2006) investigated experimentally and analytically forced convection heat transfer properties in high porosity open-cell metal-foam-filled pipes. The main result showed that the Nusselt number rises with an increase in pore density and a decrease in metal foam porosity. **(Amori and Laibi, 2011)** investigated an electrical air heater with different aluminum foam disc thicknesses experimentally and numerically. Their experimental results showed that the Nusselt number approximately doubled when a 60 mm disc thickness was used instead of 20 mm. Numerically **(Settar et al., 2015)** investigated the thermal performance of plate heat exchangers filled with metal foam. Their results showed that the temperature profiles converge faster to the wall temperature as the thermal conductivity ratio increases. **(Bayomy et al., 2016)** studied experimentally and numerically the modification of cooling a computer processor by using aluminum foam. Their results showed that the rate of heat transfer with aluminum foam rises with an increase in Reynolds number, which is accomplished with a rise in pumping power due to an increase in pressure drop across the aluminum foam.

An experimental investigation of forced convection in a channel with metal foam blocks was conducted by **(Nima and Hajeej, 2016)**. Their results showed that an increase in heat flux, Reynolds number, and pore density led to an increase in the mean Nusselt number, which improved by 80% in all cases with metal foam compared to the empty case. **(Al-Athel, 2017)** Conducted a numerical investigation to study the impact of multi-metal foam fins on the thermal resistance and efficiency of the heat sink. The efficiency improved with an increase in the number and height of metal foam fins. Convective heat transfer was considered by **(Nazari and Toghraie, 2017)** In a sinusoidal duct with a porous medium. They found that an increase in the Reynolds number led to an increase in the Nusselt number and the convection heat transfer coefficient.

(Baragh et al., 2018) Evaluated heat transfer enhancements in the circular channel filled with porous media. Their findings indicated that circular-shaped porous regions demonstrate turbulent flow conditions with excellent thermal performance. **(Kotresha and Gnanasekaran, 2019)** evaluated numerically the convection heat transfer in a rectangular channel occupied completely by aluminum foam. Many configurations were analyzed, and they found that the filled channel with metal foam has a higher Nusselt number and friction factor. Used FLUENT to simulate forced convection heat transfer through a porous graded material with a specified number of PPI. They found that graded PPI reduced friction compared to high-pore-density metal foam. **(Zhong et al., 2020)** examined numerically and experimentally forced convection heat transfer on microchannel heat sinks with copper

foam fins in various geometric forms, 110 PPI, and 95% porosity. They showed that the strip metal foam bonded to the copper plate had the largest heat transfer impact.
In square ducts filled with porous material, **(Bibin and Jayakumar, 2020)**conducted a study of the pressure drop and convective heat transfer. Their results indicate that porous addition enhances the heat transfer, while the pressure drop is minimized with a reduction in thickness. A computational analysis studied heat transfer and fluid dynamics in a sinusoidal parallel-plate heat exchange system, including metal foam in diverging parts **(Arasteh et al., 2020)**. According to their results, the usage of metal foam resulted in a 19 percent rise in the rate of heat transfer and reduction of the thermal boundary layer. LTNE and LTE were used by **(Li et al., 2020)** to find the difference in temperature between the metal foam and the working fluid in a porous heat sink. The solid-fluid temperature difference quadrupled at 15 PPI compared to 50 PPI. **(Jasim et al., 2021)** Numerically investigated the thermophysical properties of metallic foam-wrapped array heat exchangers. The result showed that the metal foam heat exchanger with 5PPI outperforms 20PPI because of an increase in pumping power with PPI increase.
(Hmad and Dukhan, 2021a) introduced a new design for fuel-cell stacks. They replaced the fuel cells with aluminum plates and metal foam. They suggested that their new design can be used in the cooling process for fuel-cell stacks because of its suitable pumping power. **(Banerjee and Paul, 2022)** analyzed PPI impact on thermal activity in a porous conduit with various porosities. They found that metal foam with a higher PPI at a given porosity has a higher Nusselt number. **(Narkhede and Gnanasekaran, 2024)** studied pressure loss in a rectangular channel filled partially with a metal foam block with varied blockage ratios (total height to local height). They found that the pressure drop rises with a rise in PPI, blockage ratio, and flow velocity.
From the literature above, it is clear that the heat transfer is enhanced with the use of metal foam. However, this enhancement is accomplished with an increase in power consumption as a result of an increase in pressure drop through this metal foam. In this study, convective heat transfer in a rectangular channel that is filled with gradient PPI copper foam is achieved. Two gradient arrangements are compared with two traditional cases to analyze the thermal performance and pressure drop through them. This work aims to reduce the losses with the gradient PPI and increase the heat transfer, then improve P.F. ANSYS FLUENT 20.0 program is utilized to solve the governing equations to obtain the temperature distribution, friction factor, Nusselt number, and performance factor. The model of **(Nima and Hajeej, 2016)** is taken as a starting point for this study.

2. METHODS

2.1 Physical Model

The simplified schematic for this problem is a (250×100) mm^2 rectangular channel filled with 97% porosity copper metal foam, as shown in **Fig. 1**. The bottom plate is subjected to a fixed heat flux (450-6000) W/m^2. **Table 1** lists the thermophysical properties of air and copper at 34 °C. **(Holman, 2002; Cengel and Ghajar, 2019)**.

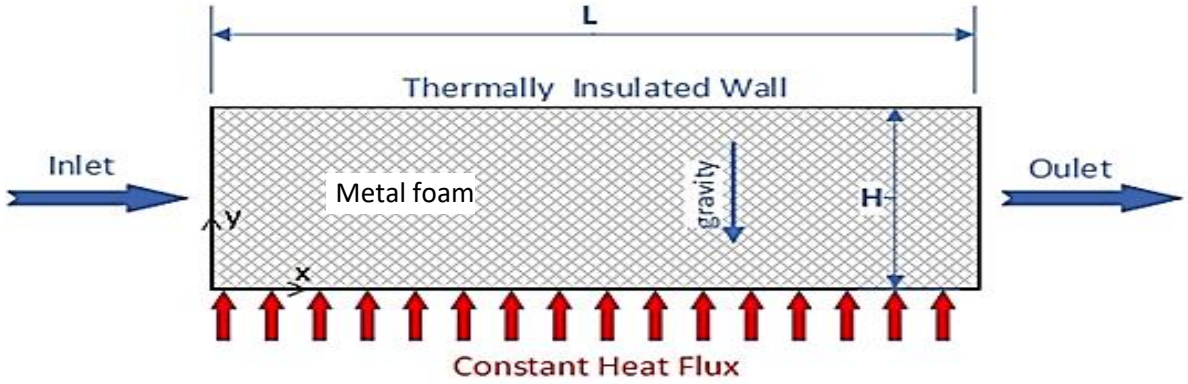

Figure 1. A systematic physical model with one block of metal foam.

Table 1. Thermophysical properties for copper and air **(Holman, 2002; Cengel and Ghajar,2019).**

Material	Thermal Conductivity (W/m.K)	Specific Heat (J/kg. K)	Density (kg/m^3)	Viscosity (kg/m.s)
Copper	386	383.1	8954	---
air	0.026	1006.03	1.167	1.5825×10^{-5}

The copper foam filled the channel with four different arrangements. In cases A and B, the channel is filled by one piece of 10 and 40 PPI, respectively. In cases C and D, the copper metal foam in the rectangular channel is divided into three blocks, each block (83×100) mm, as illustrated in **Table 2**. Case C has the order of PPI (40,20,10), in which the PPI is gradually decreasing horizontally. In case D, the arrangement is gradually increasing in the pattern (10,20,40) PPI, as shown in **Fig. 2**. The metal foam characteristics are listed in **Table 3**.

Table 2. Cases for study

No	Name	State
1	Empty case	without metal foam
2	Case A	(10) PPI
3	Case B	(40) PPI
4	Case C	(40-20-10) PPI
5	Case D	(10-20-40) PPI

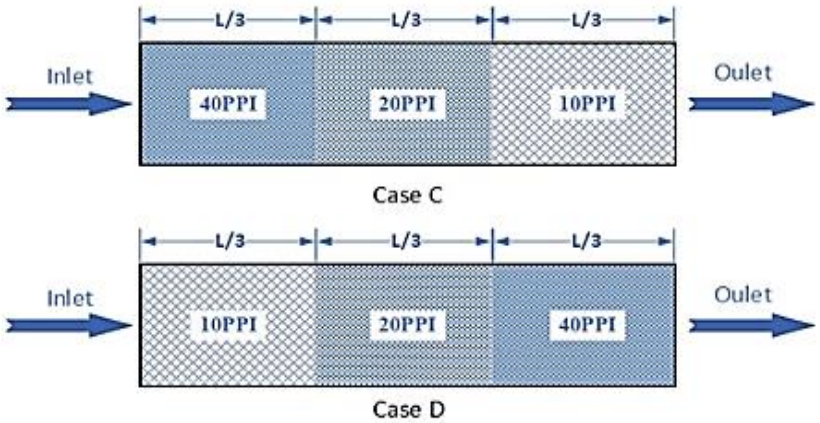

Figure 2. The copper foam block exhibits two different arrangements of pore density.

Table 3. Copper foam characteristics.

Pore per inch (PPI)	Porosity ε (%)	Permeability K (m^2)	Inertial loss coefficient C_{sf} (1/m)	Surface area density a_{sf} (1/m)
40	97	2.731×10^{6}	150.92	2838.58
20	97	1.092×10^{-5}	75.46	1419.29
10	97	4.361×10^{-5}	37.729	709.65

Inlet air flows through a channel with a velocity range from (0.048 to 0.5) m/s, which represents (200-2100) Reynolds number at 34 ^{o}C, and the pressure at the outlet section was set to the atmospheric pressure.

2.2 Assumptions

Several assumptions are given to simplify the difficulty of solving the governing equations of heat transfer and fluid flow, including the continuity, momentum, and energy equations. They are:

1. The flow is supposed to be two-dimensional, incompressible, laminar, fully developed, and in a steady state.
2. The thermophysical properties of air are assumed to remain constant.
3. The copper foam is a porous medium that is isotropic and homogenous.
4. Heat generation, radiation, and viscous dissipation are negligible.
5. The Darcy-Forchheimer extended Brickman equations are employed with LTNE.

2.3 Governing Equation

For rectangular channels filled with copper metal foam, there is one set of differential equations governing the fluid flow and heat transfer, or energy in the metallic foam. The Forchheimer-extended Darcy model is suggested to describe the momentum equation, while the two-equation non-equilibrium heat transfer model is used to describe the energy equations for both the fluid and solid phases. **(Yang et al., 2011; Gangapatnam et al., 2018; Ke et al., 2023)**.

Continuity equation:

$$Partial\frac{\partial u}{\partial x}+\frac{\partial v}{\partial y}=0 \tag{1}$$

Momentum equation:

$$\frac{\partial_P}{\partial x}+\frac{\mu\partial^2 u}{\varepsilon\partial x^2}-\frac{\mu}{k}u-\frac{\rho\, c_F}{\sqrt{k}}u^2=0 \tag{2}$$

$$\frac{\partial_P}{\partial y}+\frac{\mu\partial^2 v}{\varepsilon\partial y^2}-\frac{\mu}{k}v-\frac{\rho\, c_f}{\sqrt{k}}v^2=0 \tag{3}$$

Fluid energy equation:

$$^{\text{Open}}k_{fe}\left[\frac{\partial^2 T_f}{\partial y^2}+\frac{\partial^2 T_f}{\partial x^2}\right]+h_{sf}\ \sigma\left(T_s-T_f\right)=\rho C_P\left[\frac{\partial(uT_f)}{\partial x}+\frac{\partial(vT_f)}{\partial y}\right] \tag{4}$$

Solid energy equation:

$$k_{Se}\left[\frac{\partial^2 T_S}{\partial y^2}+\frac{\partial^2 T_S}{\partial x^2}\right]+h_{sf}\,\sigma\left(T_f-T_s\right)=0 \quad (5)$$

The thermal connection between the metal foam surface and the working fluid is important in construction, with the governing equation. Fluid and solid effective thermophysical properties and metal foam characteristics are estimated by the following equations. (**Lu et al., 2006; Xu et al., 2015**).

Interfacial heat transfer coefficient

$$h_{sf}=\begin{cases} 0.76Re_d^{0.4}p_r^{0.37}\frac{k_f}{d}\,(1\le Re_d\le 40) \\ 0.52Re_d^{0.5}p_r^{0.37}\frac{k_f}{d}\,(40\le Re_d\le 10^3) \\ 0.26Re_d^{0.6}p_r^{0.37}\frac{k_f}{d}\,(10^3\le Re_d\le 2*10^5) \end{cases} \quad (6)$$

Pore diameter

$$d_P=\frac{0.0254}{PPI} \quad (7)$$

Fiber diameter

$$d_f=d_p.1.18\sqrt{\frac{1-\varepsilon}{3\pi}}\left[1-exp\left(\frac{\varepsilon-1}{0.04}\right)\right]^{-1} \quad (8)$$

Permeability

$$K=\frac{(d_P)^2*(\varepsilon)^3}{150*(1-\varepsilon)^2} \quad (9)$$

Viscous resistance

$$\alpha=\frac{1}{k} \quad (10)$$

Inertial coefficient

$$c_F=\frac{3.5(1-\varepsilon)}{d_p\varepsilon^3} \quad (11)$$

Interfacial surface area

$$\sigma\ =3\pi d_f\left[1-exp\left(\frac{1-\varepsilon}{0.04}\right)\right]/\,(0.59\,dp)^2 \quad (12)$$

The calculation of Re is dependent on the hydrodynamic diameter, density, dynamic viscosity, and fluid velocity at the entrance. **(Li et al., 2017).**

Hydraulic diameter

$$D_h=\frac{(2wh)}{(w+h)} \quad (13)$$

Mean diameter

$$d = \left(1 - exp\left(\frac{1-\varepsilon}{0.04}\right)\right) \quad (14)$$

Reynolds number

$$Re = \frac{\rho u D_h}{\mu} \quad (15)$$

Reynolds number with a mean diameter

$$Re_d = \frac{\rho u d}{\mu} \quad (16)$$

The integration of the bulk temperature (T_b) is taken into consideration:

$$T_b = \frac{\int_0^H T u \, dy}{\int_0^H u \, dy} \quad (17)$$

The local heat transfer coefficient at any *x* with flow direction is:

$$h(x) = \frac{q''}{T_w - T_b} \quad (18)$$

Average heat transfer coefficient

$$h = \frac{1}{L}\int_0^L h_{(x)} \, dx \quad (19)$$

Average Nusselt number

$$Nu = \frac{h D_h}{k} \quad (20)$$

Friction factor (**Bağc and Dukhan, 2018**)

$$f = \frac{2\Delta p D_h}{\rho_f u_0^2 L} \quad (21)$$

Performance factor (**Cekmer et al., 2012; Ali and Ghashim, 2023**)

$$P.F. = \frac{(Nu/Nu_e)}{(f/f_e)^{1/3}} \quad (22)$$

2.4 Boundary Condition

Velocity and temperature boundary conditions are:

At inlet: $u = u_{in}$, v $= 0$ and $T_f = T_{in}$, $\frac{\partial T_s}{\partial x} = 0$

At outlet: $p = 0$ and $\frac{\partial T_f}{\partial x} = \frac{\partial T_s}{\partial x} = \frac{\partial u}{\partial x} = \frac{\partial \mathrm{v}}{\partial x} = 0$

Heated wall: q˝$= -k_f \frac{\partial T_f}{\partial y} = -k_S \frac{\partial T_S}{\partial y}$, $u = v = 0$

Wall insulation $\frac{\partial T_f}{\partial y} = \frac{\partial T_S}{\partial y} = 0$, $u = v = 0$

3. THE NUMERICAL SOLUTION

The ANSYS FLUENT 20.0 program utilizes the LTNE model to obtain two-dimensional numerical solutions for heat transfer and flow through porous channels. A Simple algorithm is used to match the pressure with velocity through the flow, while the determination of momentum and energy equations is done by applying the second-order upwind computation scheme. User-defined function codes are applied to interpret the governing equations of the interfacial heat transfer coefficient h_{sf}.

3.1 Mesh Independence

The solution accuracy always depends on the size and type of the mesh. The grid sensitivity is conducted to determine the optimum mesh size that produces stable results for the current model. Many computational grids are tested to choose the suitable mesh elements, as shown in **Table 4**. Based on the number of elements, **Fig. 3** illustrates the variety of average heat transfer coefficients for Case D at Re=1600 and q" = 6000W/m^2. The grid size for (1185159 elements) is chosen as the optimum size for all cases.

Table 4. Grid independent study for (10-20-40) PPI metallic foam, Ɛ=0.97 at Re=2100 with heat flux=3000 W/m^2.

		M_1	M_2	M_3	M_4	M_5	M_6
Element size		0.00025	0.0002	0.00015	0.000145	0.00014	0.000135
Number of Elements		399603	623687	1107488	1185159	1269838	1365811
$T_{ave\ (K)}$		342.493	342.106	341.563	341.5	341.44	341.378
ΔP		41.56	41.575	41.588	41.591	41.594	41.597
Deviation (%)	T_{ave}	--	0.112995	0.158722	0.018444	0.017569	0.018158
	ΔP	--	0.036079	0.031259	0.007213	0.007212	0.007212

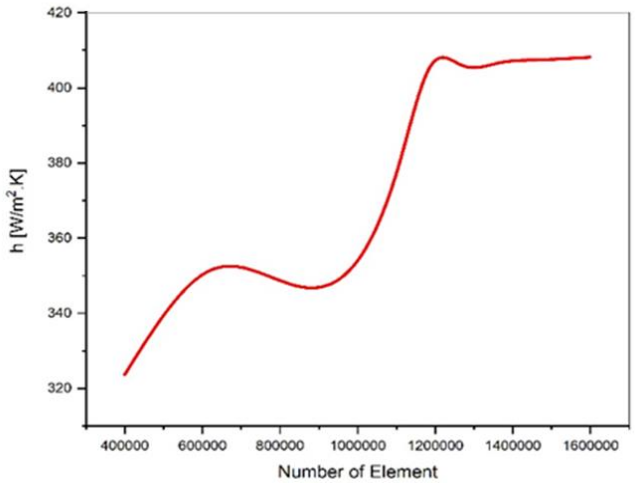

Figure 3. Average heat transfer coefficient via several elements.

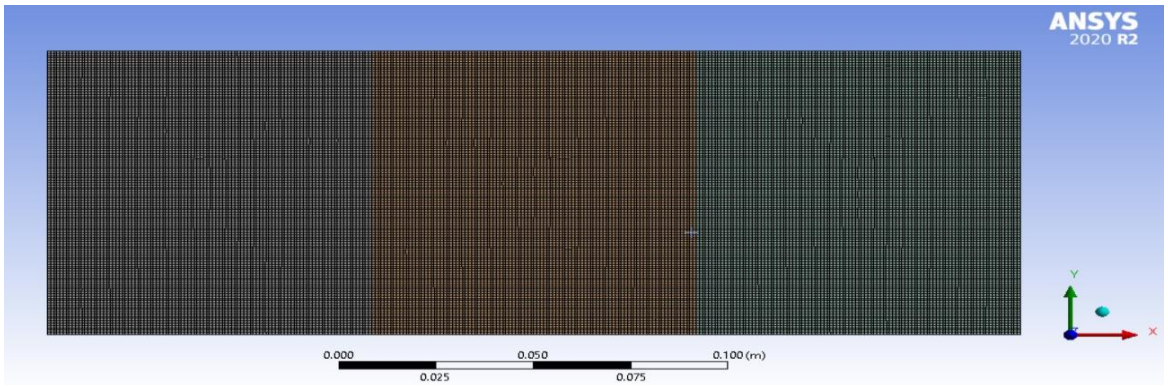

Figure 4. Mesh generation of metal foam.

3.2 Verification

The present model is used to solve the problem of **(Hmad and Dukhan, 2021b)** To show its validity. A simulation is conducted for 40 PPI and heat flux 1.5 W/cm^2 with velocity from 0.25 to 3 m/s. **Fig. 5** shows the deviation of the obtained values of the heat transfer coefficient **(Hmad and Dukhan, 2021b)**. The deviation between the results is less than 1 %. This indicates that the model is valid and can be used to obtain more results for thermal performance and pressure drop.

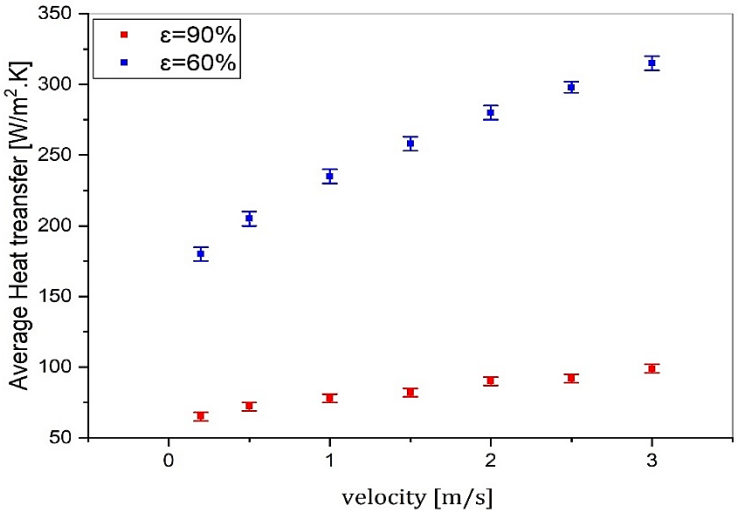

Figure 5. The present study verification with **(Hmad and Dukhan, 2021b)** At two porosities (90% and 60%) and constant heat flux (1.5 W/cm^2), and with velocity from 0.25 to 3 m/s.

4. RESULTS AND DISCUSSION

4.1 Temperature Distribution

Fig. 6 shows the impact of Re on the wall temperature distribution at q'' = (3000W/m^2) for both case C and D. For case C, the wall temperature increases gradually with flow direction as the thermal boundary layer grows. For case D, the general behavior is that the temperature rises along each section. However, it drops at the inlet of the second and third

sections. This is due to the pore density's arrangement (a gradual increase from 10 to 40 PPI) in these sections, which decreases the thermal boundary layer thickness.
In both cases, increasing the Re drops the wall temperature at each location in the channel at one heat flux. As the Re increases, the thermal boundary layer drops along the heated wall at each location.
The temperature of the wall rises at each location as the heat flux increases because the buoyancy effect also rises, which leads to a faster rise in the thermal boundary layer thickness along the flow direction, as shown in **Fig. 7**. Both cases C and D behave similarly when the heat flux increases. However, case D has a lower wall temperature due to a better pore density arrangement, which causes a better heat transfer from the heated surface to the working fluid.

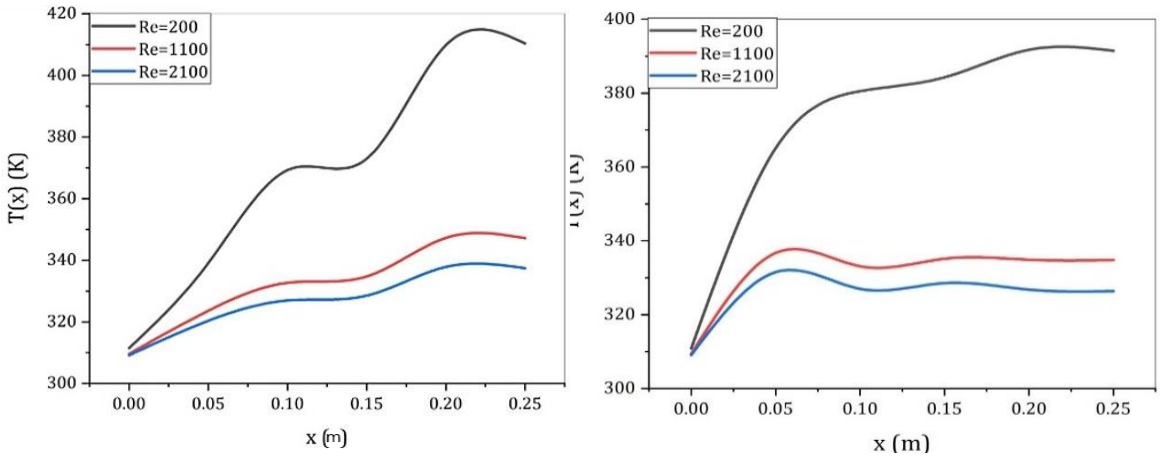

Figure 6. The local wall Temperature variation with Reynolds number at q'' =3000 (W/m^2) and (a) case C (40-20-10) PPI and (b) case D (10-20-40) PPI.

4.2 Local Heat Transfer Coefficient

Fig. 8 shows the impact of Re on the local heat transfer coefficient at q'' =(3000W/m^2). It is clear that for a certain value of Re and q, the local heat transfer coefficient along the rectangular channel decreases gradually along the channel. This decrease is caused by the pore density's arrangement along the channel, which leads to a decrease in air mixing and an increase in thermal boundary layer resistance.

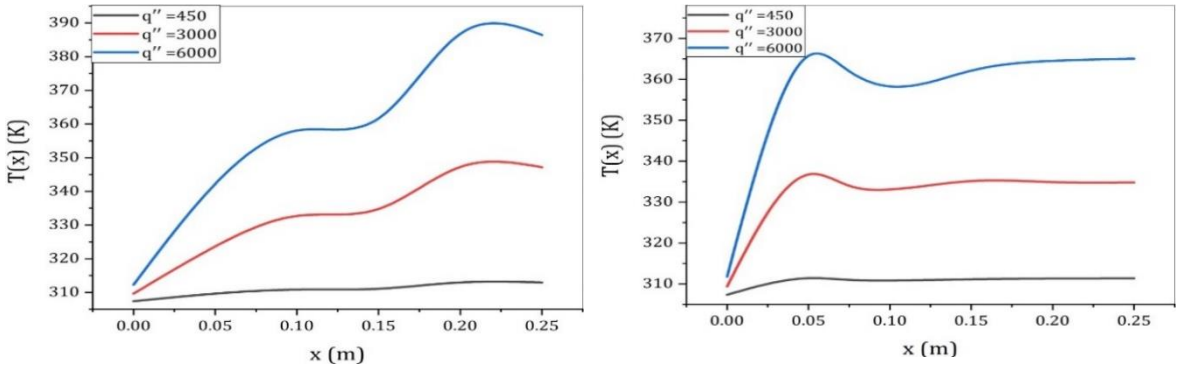

Figure 7. The local wall Temperature variation with heat flux at Re =1100 for (a) case C (40-20-10) PPI and (b) case D (10-20-40) PPI.

However, for case D, the local heat transfer coefficient along the rectangular channel decreases gradually in the first section only. Then, it continues to rise in the remaining sections as the wall temperature decreases in these sections.
At the same time, the increase in the Reynolds number leads to a decrease in the resistance of the thermal boundary layer. This is due to the dominance of the incoming cold fluid, resulting in greater mixing currents and higher values of the local heat transfer coefficient. This effect is particularly pronounced in the first section, which is the closest to the inlet for both cases.

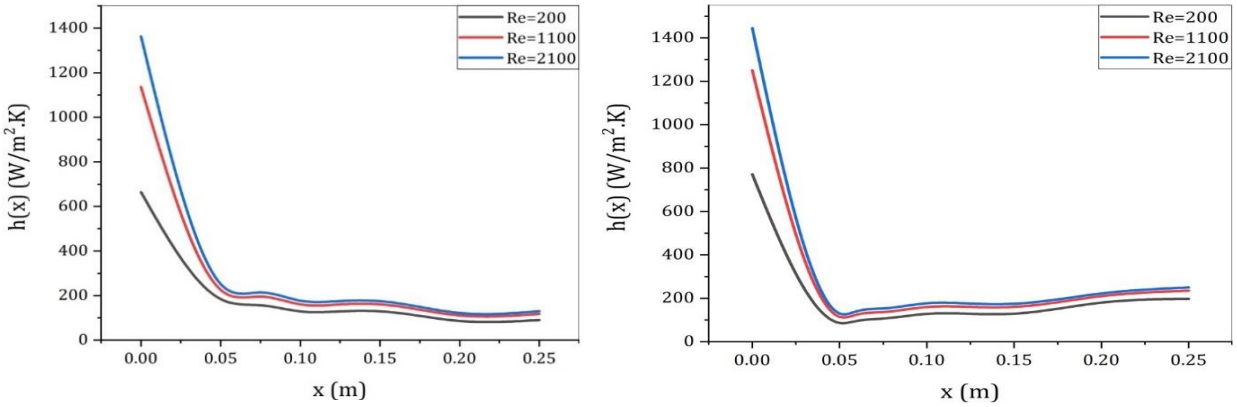

Figure 8. The variation of local heat transfer coefficient with Reynolds number at q'' =3000 (W/m²) and (a) case C (40-20-10) PPI and (b) case D (10-20-40) PPI.

Fig. 9 shows that the heat transfer coefficient at the inlet is very high and it decreases rapidly with the flow direction through the first quarter. Then, it decreases gradually towards the outlet in case C, while it increases gradually in case D. This behavior is a result of the PPI gradient. In case C, the flow begins with high resistance, which leads to a reduction in the flow momentum and increases the local temperature. In case D, the PPI is graduated from low to high PPI, which allows more air to flow adjacent to the wall and reduces the local temperature. Also, **Fig. 9** shows the impact of heat flux on the local heat transfer coefficient at Re =1100. As the heat flux rises, the local heat transfer coefficient remains constant.

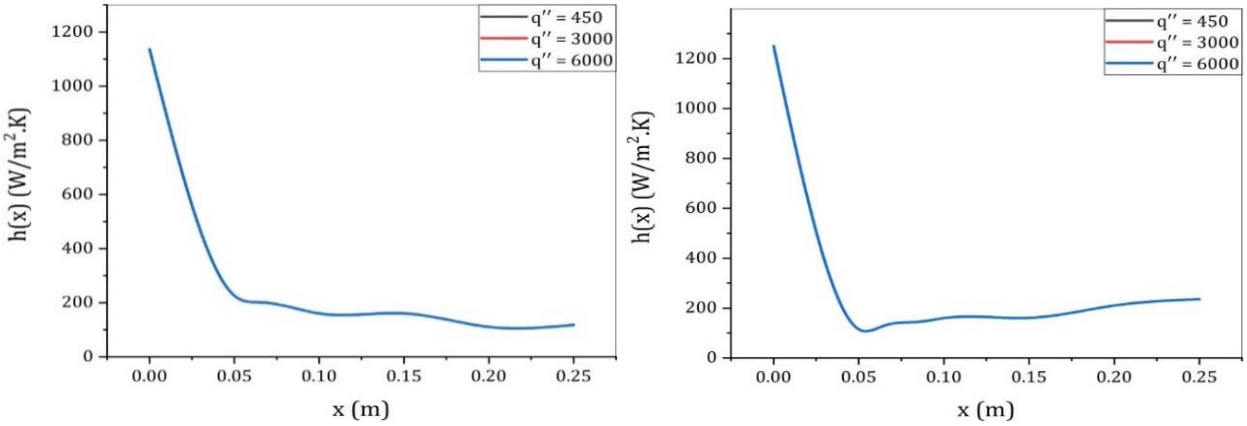

Figure 9. The variation of local heat transfer coefficient with heat flux at Re=1100 (a) case C (40-20-10) PPI, (b) case D (10-20-40) PPI.

It may be credited that for larger heat flux, the buoyancy currents grow, and the thermal boundary layer grows more quickly. This led to a fixed temperature difference between the bulk temperature of the working fluid and the temperature of the heated wall at each location in the flow direction.

4.3 Average Nusselt Number

Fig. 10 presents the impact of Re on the average Nusselt number for all cases at a heat flux of 3000 W/m^2. The Nusselt number improves with an increase in Re for all cases because of an increase in flow momentum. Adding metal foam led to the enhancement of the heat transfer process; therefore, the Nusselt number also increased. This enhancement in heat transfer increases with an increase in the pore density of the metal foam, leading to an expansion in the surface area of heat transfer. For Case B, the average Nusselt number increases by 87.28% and 18.5%, 12.9%, and 5.5% compared with the empty case, cases A, C, and D, respectively, at Re=2100. Case D exhibits a higher average Nusselt number than Case C, which can be attributed to an arrangement in pore density that enhances the breaking of the thermal boundary layer. The increase is 8% compared to case C.
The four tables of case B return to the higher turbulence and strong mixing through the metal foam, which causes a greater reduction in the boundary layer resistance. This decreases the temperature difference between the hot surface and the airflow and increases the local heat transfer coefficient. **Table 5.** shows the Nusselt number variation with the Reynolds number for all cases with constant heat flux.

Table 5. The average Nusselt number with variation in the Reynolds number (2100 to 200) and constant heat flux (3000 W/m^2).

Reynolds number	Nu				
	Empty case	Case A	Case B	Case C	Case D
200	50.5	505.1	583.6	535.5	623.7
600	78.1	661.8	821.9	690.1	789.4
1100	101.8	758.6	931.8	798.0	889.7
1600	120.1	820.5	1006.1	871.6	953.9
2100	135.7	865.9	1062.1	925.9	1001.5

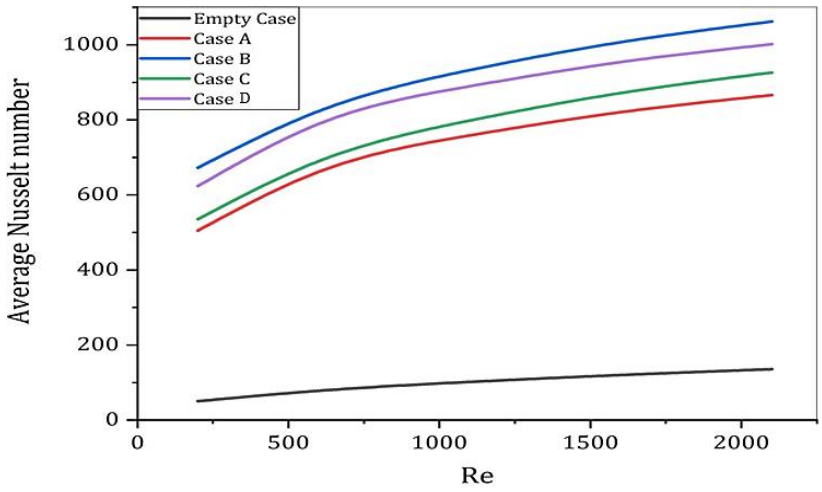

Figure 10. Average Nusselt number variation with Reynolds number (200 to 2100) at q'' =3000(W/m^2).

4.4 Pressure Drop

Fig. 11 illustrates the variation of pressure drop with Re for all cases at q'' =3000 (W/m^2). It turns out that cases D and C have the same pressure drop for all values of Re because the structure has equal hydraulic properties of the metal foam in cases C and D, resulting in equal pressure drop in both cases. A high flow obstruction occurs when the flow passes through metal foam, and this resistance increases more with PPI increase. In the case of B, there is a significant increase in the pressure drop compared to other cases, namely by approximately 95.7%, 10.9%, and 19.92% compared with the empty case, case D, and case A, respectively. **Table 6**. shows the pressure drop variation with Reynolds number for all cases with constant heat flux.

Table 6. The pressure drops with variation in the Reynolds number (2100 to 200) and constant heat flux (3000 W/m^2).

Reynolds number	Pressure drop				
	Empty case	Case A	Case B	Case C	Case D
200	4	14	25.2	18.5	18.5
600	8	52	67.2	57.6	57.6
1100	12	104	136	109.6	109.6
1600	16	156	196	171.0	171.0
2100	20	208	252	228.0	228.0

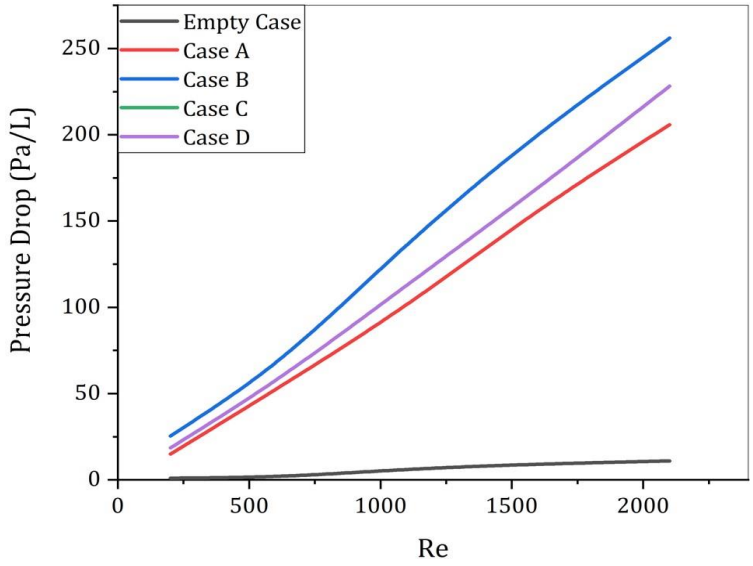

Figure 11. Pressure drops vary with Reynolds (200 to 2100) at q'' =3000 (W/m^2).

4.5 Friction Factor

Fig. 12 illustrates the variety of friction factors with Re for all four cases. It is imperative to note that the friction factor drops with Re rise. The increase in pore density increases the friction factor because when the pores per inch in the metal foam are increased, it leads to highly turbulent fluid, and this increase in pore density increases the shear stress because of an increase in the number of pores which means increase in contact area between the solid and air. Case B shows a higher friction factor than cases A, C, and D, with values equal to

which should be 68.38%, 9.5%, and 17.5%, greater than in the empty case, cases D and A, respectively. **Table 7.** shows the friction factor variation with Reynolds number for all cases with constant heat flux.

Table 7. The friction factor with variation in the Reynolds number (2100 to 200) and constant heat flux (3000 W/m²).

Reynolds number	Friction factor				
	Empty case	Case A	Case B	Case C	Case D
200	202.6	709.1	1276.4	938.2	938.2
600	44.8	291.5	376.7	323.2	323.2
1100	20.1	174.2	227.8	183.8	183.8
1600	12.6	123.4	155.1	135.3	135.3
2100	9.1	95.5	115.7	104.6	104.6

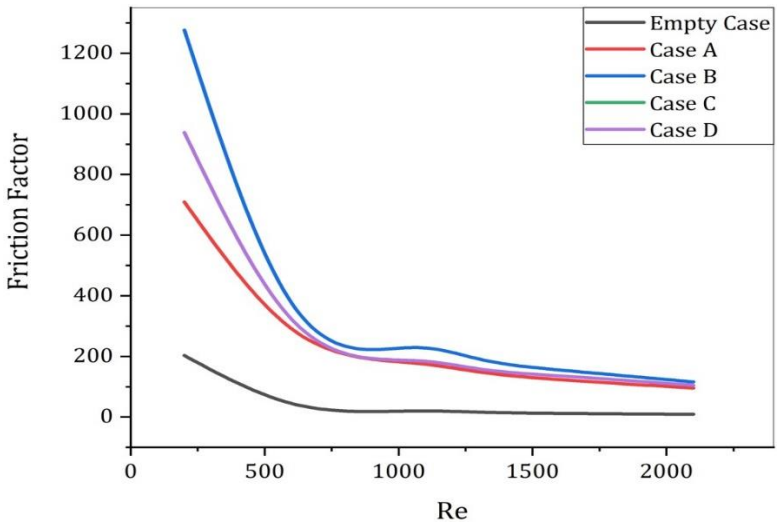

Figure 12. Friction factor variation with Reynolds number (200 to 2100) at q'' =3000 (W/m²).

4.6 Performance Factor

Fig. 13 shows the impact of varying Reynolds numbers on performance factors for all four cases at 3000 W/m². With each rise in the Reynolds number, the thermal performance factor decreases considerably. For all cases, the performance factor drops with Re decrease, which means the percentage increase in friction is more than the heat gain ratio. Case D demonstrates the highest performance factor in the rectangular channel when compared to other cases with constant porosity. This is due to a larger percentage increase in the ratio between the Nusselt number with metal foam and without metal foam, compared with the ratio between the friction factor with and without metal foam. This behavior is caused by the friction factor in case D being lower than in case B, and the heat transfer in case D being higher than in case A. Moreover, the Nusselt number in case D is slightly higher than that in case C, and the friction factor is equal in both cases. But the friction factor gradient in case D is less steep than in case C, and because of this small slope, the fluid flows in case D with less resistance than in case C.

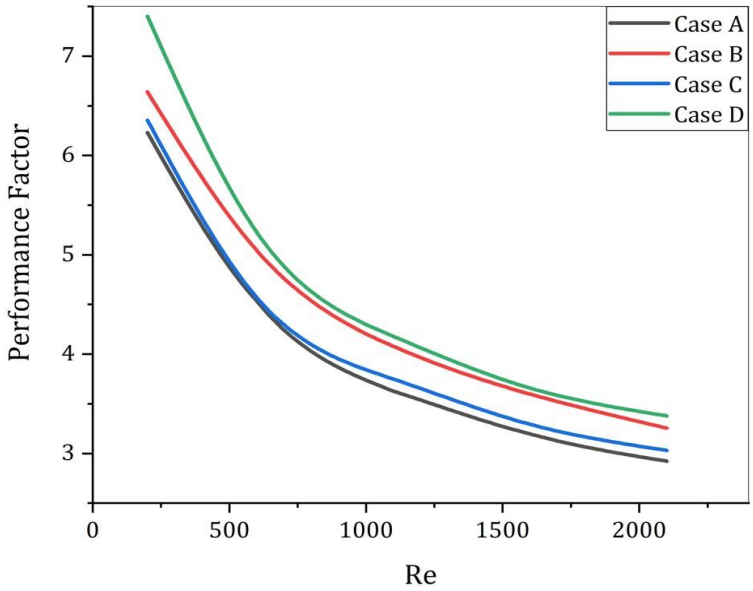

Figure 13. Performance factor variation with Reynolds number (200 to 2100) at q'' =3000 (W/m²).

5. CONCLUSIONS

ANSYS FLUENT 20.0 was applied to achieve a two-dimensional numerical simulation for convective heat transfer in a porous rectangular channel with gradient PPI. The present investigation has yielded the following significant findings:

1- Adjacent to the Re increase, the local heat transfer coefficient and Nu increase. In contrast, the heat flux has a slight effect.
2- Both the gradient cases (C and D) have pressure drop and heat transfer coefficients between cases A and B, however, case D has a higher heat transfer coefficient compared to Case C with the same pressure drop.
3- It can be said that Case D is the best case since it has a P.F. with 10% greater than that in Case B.

The obtained results justify expanding future studies to study different channel shapes or the use of metal foam from other metals, such as aluminum, nickel, or other metal foam formations. This is important in engineering applications to obtain an ideal, highly efficient design with lower production costs.

NOMENCLATURE

Symbol	Description	Symbol	Description
c_F	Viscous resistance, 1/m	PF	Performance factor
c_p	Specific heat, J/kg. K	q''	Heat flux, W/m²
D_h	Hydraulic diameter, m	Re	Reynolds number
d_f	Fiber diameter, m	T	Temperature, °C
d_m	Mean diameter, m	u	Velocity component in x-direction, m/s
d_p	Pore diameter, m	v	Velocity component in y-direction, m/s
f	Friction factor	x	length, m

$h_{(x)}$	Heat transfer coefficient, W/m².℃	k_f	Fluid thermal conductivity
h_{sf}	Interfacial heat transfer coefficient, W/m². ℃	k_{fe}	Fluid effective thermal conductivity
H	Duct height, m	k_s	Solid thermal conductivity
k	Thermal conductivity, W/m. K	k_{se}	Solid effective thermal conductivity
K	Permeability, m²	σ	Specific surface area, 1/m
L	Duct length, m	α	Inertia resistance
LTE	local thermal equilibrium	Δ	Drop
LTNE	local thermal nonequilibrium	∂	Differential
Nu	Nusselt number	ε	Porosity
Nu_e	Nusselt number of empty cases	μ	Fluid dynamic viscosity, N/s.m²
P	Pressure, pa	ρ	Density, kg/m³
PPI	Pore per inch		

Acknowledgements

This work was supported by the University of Baghdad, College of Engineering in Baghdad, Iraq.

Credit Authorship Contribution Statement

Mohammed H. Hasan: Conceptualization, writing original draft, analysis, and interpretation of results; Raed G. Saihood: Conceptualization, writing, review, and supervision.

Declaration of Competing Interest

The authors declare that they have no known competing financial interests or personal relationships that could have appeared to influence the work reported in this paper.

REFERENCES

Akbar, I., Rawani, D., Rusmaryadi, H., King, M.L., Fatoni, Z., Aziz, A.M.A., Prakoso, A.T., Basri, H., Mataram, A. and Pramadhony, 2024. Analysis of the effect of tortuosity porous heatsink on forced convection heat transfer. *Journal of Advanced Research in Numerical Heat Transfer*, 16(1), pp. 57–69. https://doi.org/10.37934/arnht.16.1.5769.

Al-Athel, K.S., 2017. Computational assessment of the heat transfer coefficient under forced convection of multiple metal foam fins heat sinks. *Arabian Journal for Science and Engineering*, 42(11), pp. 4853–4861. https://doi.org/10.1007/s13369-017-2656-2.

Ali, R.M.K. and Ghashim, S.L., 2023. Numerical analysis of the heat transfer enhancement by using metal foam. *Case Studies in Thermal Engineering*, 49, 103336. https://doi.org/10.1016/j.csite.2023.103336.

Ali, S.A. and Rasheed, S.A., 2024. Experimental investigation of forced convection in plain or partly inserted square channel with porous media. *Journal of Engineering*, 30(04), pp. 99–117. https://doi.org/10.31026/j.eng.2024.04.07.

Amori, K.E. and Laibi, H.A., 2011. Experimental and numerical analysis of electrical metal foam heater. *Energy*, 36(7), pp. 4524–4530. https://doi.org/10.1016/j.energy.2011.03.062.

Arasteh, H., Mashayekhi, R., Ghaneifar, M., Toghraie, D. and Afrand, M., 2020. Heat transfer enhancement in a counter-flow sinusoidal parallel-plate heat exchanger partially filled with porous media using metal foam in the channels' divergent sections. *Journal of Thermal Analysis and Calorimetry*, 141(5), pp. 1669–1685. https://doi.org/10.1007/s10973-019-08870-w.

Bağc, Ö. and Dukhan, N., 2018. Impact of pore density on oscillating liquid flow in metal foam. *Experimental Thermal and Fluid Science*, 97, pp. 246–253. https://doi.org/10.1016/j.expthermflusci.2018.04.020.

Banerjee, A. and Paul, D., 2022. Heat transfer analysis using a duct filled with metal foams. *Journal of Thermal Engineering*, 8(4), pp. 529–537. https://doi.org/10.18186/thermal.1149655.

Baragh, S., Shokouhmand, H., Ajarostaghi, S.S.M. and Nikian, M., 2018. An experimental investigation on forced convection heat transfer of single-phase flow in a channel with different arrangements of porous media. *International Journal of Thermal Sciences*, 134, pp. 370–379. https://doi.org/10.1016/j.ijthermalsci.2018.04.030.

Bayomy, A.M., Saghir, M.Z. and Yousefi, T., 2016. Electronic cooling using water flow in aluminum metal foam heat sink: Experimental and numerical approach. *International Journal of Thermal Sciences*, 109, pp. 182–200. https://doi.org/10.1016/j.ijthermalsci.2016.06.007.

Bibin, K.S. and Jayakumar, J.S., 2020. Thermal-hydraulic characteristics of square ducts having porous material inserts near the duct wall or along the duct center. *International Journal of Heat and Mass Transfer*, 148, 119079. https://doi.org/10.1016/j.ijheatmasstransfer.2019.119079.

Cekmer, O., Mobedi, M., Ozerdem, B. and Pop, I., 2012. Fully developed forced convection in a parallel plate channel with a centered porous layer. *Transport in porous media*, 93(1), pp. 179–201. https://doi.org/10.1007/s11242-012-9951-x.

Gangapatnam, P., Kurian, R. and Venkateshan, S.P., 2018. Numerical simulation of heat transfer in metal foams. *Heat and Mass Transfer/Waerme- und Stoffuebertragung*, 54(2), pp. 553–562. https://doi.org/10.1007/s00231-017-2149-6.

Hmad, A.A. and Dukhan, N., 2021a. A Cooling design for an end cell in fuel-cell stack using forced airflow in metal foam: Modelling and experiment. *In: IOP Conference Series: Materials Science and Engineering*. 12008. https://doi.org/10.1088/1757-899X/1190/1/012008.

Hmad, A.A. and Dukhan, N., 2021b. Cooling design for PEM fuel-cell stacks employing air and metal foam: simulation and experiment. *Energies*, 14(9), 2687. https://doi.org/10.3390/en14092687.

Holman, J.P., 2002. *Heat transfer*. 9th ed. New York: McGraw-Hill.

Jasim, N.M., Fayyadh, E.M. and Hasan, M.R., 2021. Numerical study on the effect of geometrical parameters on the thermal-hydraulic performance of the metal foam heat exchanger. *In: IOP Conference Series: Materials Science and Engineering*. 12112. https://doi.org/10.1088/1757-899X/1094/1/012112.

Ke, H., Zhou, X., Liu, T., Wang, Y. and Wang, H., 2023. Numerical study of heat and mass transfer in the original structure and homogeneous substitution model for three-dimensional porous metal foam. *Energies*, 16(3), 1114. https://doi.org/10.3390/en16031114.

Kopanidis, A., Theodorakakos, A., Gavaises, E. and Bouris, D., 2010. 3D numerical simulation of flow and conjugate heat transfer through a pore-scale model of high porosity open-cell metal foam.

International Journal of Heat and Mass Transfer, 53(11–12), pp. 2539–2550. https://doi.org/10.1016/j.ijheatmasstransfer.2009.12.067.

Kotresha, B. and Gnanasekaran, N., 2019. Analysis of forced convection heat transfer through graded PPI metal foams. *In: Numerical Heat Transfer and Fluid Flow: Select Proceedings of NHTFF 2018*. pp. 151–158. https://doi.org/10.1007/978-981-13-1903-7_18.

Li, Y., Gong, L., Lu, H., Zhang, D. and Ding, B., 2020. Thermal modeling and analysis of metal foam heat sink with thermal equilibrium and non-equilibrium models. *Computer Modeling in Engineering & Sciences*, 123(2), pp. 895–912. https://doi.org/10.32604/cmes.2020.09009.

Li, Y., Gong, L., Xu, M. and Joshi, Y., 2017. Thermal performance analysis of biporous metal foam heat sink. *Journal of Heat Transfer*, 139(5), 52005. https://doi.org/10.1115/1.4035999.

Lu, W., Zhao, C.Y. and Tassou, S.A., 2006. Thermal analysis on metal-foam filled heat exchangers. Part I: Metal-foam-filled pipes. *International journal of heat and mass transfer*, 49(15–16), pp. 2751–2761. https://doi.org/10.1016/j.ijheatmasstransfer.2005.12.012.

Narkhede, A. and Gnanasekaran, N., 2024. 3D numerical modelling of turbulent flow in a channel partially filled with different blockage ratios of metal foam. *Journal of Applied Fluid Mechanics*, 17(3), pp. 548–558. https://doi.org/10.47176/jafm.17.3.2189.

Nazari, S. and Toghraie, D., 2017. Numerical simulation of heat transfer and fluid flow of Water-CuO Nanofluid in a sinusoidal channel with a porous medium. *Physica E: Low-dimensional Systems and Nanostructures*, 87, pp. 134–140. https://doi.org/10.1016/j.physe.2016.11.035.

Nima, M.A. and Hajeej, A.H., 2016. Experimental investigation of convection heat transfer enhancement in horizontal channel provided with metal foam blocks. *Journal of Engineering*, 22(5), pp. 144–161.

Qu, Z., Xu, H. and Tao, W., 2012. Numerical simulation of non-equilibrium conjugate heat transfer in tubes partially filled with metallic foams. *Journal of Thermal Science and Technology*, 7(1), pp. 151–165. https://doi.org/10.1299/jtst.7.151.

Rasheed, S.A. and Abood, J.M., 2017. Force convection heat transfer from a different cross-section cylinder embedded in porous media. *Al-Nahrain Journal for Engineering Sciences*, 20(3), pp. 727–736.

Sener, M., Yataganbaba, A. and Kurtbas, I., 2016. Forchheimer forced convection in a rectangular channel partially filled with aluminum foam. *Experimental Thermal and Fluid Science*, 75, pp. 162–172. https://doi.org/10.1016/j.expthermflusci.2016.02.003.

Settar, A., Nebbali, R., Madani, B. and Abboudi, S., 2015. Numerical investigation of convective heat transfer in a plane channel filled with metal foam under local thermal non-equilibrium. *Mechanics & Industry*, 16(5), 504. https://doi.org/10.1051/meca/2015035.

Shokouhmand, H. and Emami, S.M., 2012. Experimental investigation of flow and forced convection heat transfer, in fully filled rectangular duct using porous media. *HEFAT* 2012.

Xu, H.J., Gong, L., Zhao, C.Y., Yang, Y.H. and Xu, Z.G., 2015. Analytical considerations of local thermal non-equilibrium conditions for thermal transport in metal foams. International Journal of Thermal Sciences, 95, pp. 73–87. https://doi.org/10.1016/j.ijthermalsci.2015.04.007.

Xu, H.J., Qu, Z.G., Lu, T.J., He, Y.L. and Tao, W.Q., 2011. Thermal modeling of forced convection in a parallel-plate channel partially filled with metallic foams. *ASME. J. Heat Transfer*. 133(9): 092603. https://doi.org/10.1115/1.4004209.

Yang, C., Ando, K. and Nakayama, A., 2011. A local thermal non-equilibrium analysis of fully developed forced convective flow in a tube filled with a porous medium. *Transport in porous media*, 89, pp. 237–249. https://doi.org/10.1007/s11242-011-9766-1.

Yunus Cengel and Afshin Ghajar, 2019. *Heat and Mass Transfer: Fundamentals and Applications*. 5th ed. McGraw-Hill Education.

Zhong, Z., Meng, L., Li, X., Zhang, G., Xu, Y., and Deng, J., 2020. Enhanced heat transfer performance of optimized micro-channel heat sink via forced convection in cooling metal foam attached on copper plate. *Journal of Energy Storage*, 30, 101501. https://doi.org/10.1016/j.est.2020.101501.

دراسة العددية لأنتقال الحرارة بالحمل في قناة مستطيلة مملوءة بالرغوة المعدنية متدرجة الثقوب في البوصة الواحدة

محمد حسين حسن*، رائد كاطع صيهود

قسم الهندسة الميكانيكية, كلية الهندسة, جامعة بغداد, بغداد, العراق

الخلاصة

تم استخدام الرغوة المعدنية مؤخراً في العديد من التطبيقات الهندسية مثل المجمعات الشمسية والمبادلات الحرارية وتبريد الأجهزة الإلكترونية، مما يستدعي دراسة حالات مختلفة لاستخدام الرغوة المعدنية في هذه التطبيقات. أجريت الدراسة الحالية تحليلا عدديا لخصائص انتقال الحرارة وتدفق الموائع للهواء في قناة مستطيلة مغطاة برغوة النحاس عالية المسامية. تناولت الدراسة الأداء الحراري لحالتين من كثافة المسام المتدرجة والتي تم ترتيبها على النحو (10–20–40) PPI و (40–20–10) PPI. وتمت مقارنة هذه الحالات مع حالتين أخريين لكثافة مسام ثابتة تبلغ 10 و40 فجوة في البوصة وحالة قناة فارغة. استخدم برنامج ANSYS FLUENT 20.0 نموذج Darcy-Forchheimer الموسع Brickman في مجال ثنائي الأبعاد مع نموذج عدم التوازن الحراري المحلي (LTNE) لمعادلة الطاقة للحصول على المحاكاة العددية لهذه الدراسة. تضمنت متغيرات العمل هواء ذو رقم رينولدز من 200 إلى 2100 وفيض حراري من 450 إلى 6000 واط / م2. أشارت النتائج إلى أن استخدام الرغوة المعدنية ذات الكثافة المسامية المنخفضة أدى إلى انخفاض كل من رقم نسلت وانخفاض الضغط. أظهرت كلتا حالتي التدرج رقم نسلت وعامل الاحتكاك اللذان يقعان ضمن نطاق حالات PPI الثابتة ولكن إحدى حالات التدرج تزيد من عامل الأداء بنسبة 10٪. بشكل عام، أظهر تكوين PPI من 10–20–40 معامل نقل حرارة أعلى مقارنةً بترتيب 40–20–10 PPI مع نفس انخفاض الضغط.

الكلمات المفتاحية: التدرج، الحمل الحراري، الرغوة المعدنية، المستطيل، فجوة في البوصة الواحدة.